Chemical Engineering Journal 152 (2009) 36–43

Contents lists available at ScienceDirect

Chemical Engineering Journal

journal homepage: www.elsevier.com/locate/cej

Application of urea-based SNCR to a municipal incinerator: On-site test and CFD simulation

Thanh D.B. Nguyen[a], Tae-Ho Kang[a], Young-Il Lim[a,*], Won-Hyeon Eom[b], Seong-Joon Kim[b], Kyung-Seun Yoo[b]

[a] Lab. FACS, RCCT, Department of Chemical Engineering, Hankyong National University, Gyonggi-do, Anseong-si, Jungangno 167, 456-749, Republic of Korea
[b] Department of Environmental Engineering, Kwangwoon University Seoul, Nowon-gu, Wolgye-dong 447-1, 139-701, Republic of Korea

ARTICLE INFO

Article history:
Received 14 October 2008
Received in revised form 11 March 2009
Accepted 18 March 2009

Keywords:
NO_x reduction
Selective non-catalytic reduction (SNCR)
Computational fluid dynamics (CFD)
Urea solution
Nonuniform droplet size
Incinerator

ABSTRACT

NO_x controlling in a municipal solid waste incinerator by selective non-catalytic reduction (SNCR) using urea–water solution is studied by means of computational fluid dynamics (CFD) simulation, which is validated with on-site experiments. A three-dimensional turbulent reacting flow CFD model including the reduced chemical kinetics and the reagent droplet phase is developed to predict the performance of the SNCR process installed in the incinerator. At normalized stoichiometric ratio (NSR) = 1.8, 70% NO (nitrogen oxide) reduction is obtained from on-site experiments, while 66% NO reduction is from the CFD simulation with the nonuniform droplet size. NH_3 slip obtained from the CFD simulation is in reasonable agreement with the *in-situ* experiment.

The effect of the droplet size distribution on the nitrogen oxide reduction efficiency is examined on CFD simulation results. Since the NO concentration at the SNCR exit is more dispersed in the nonuniform droplet size than in the uniform one, the nonuniform droplet size enhances mixing with the flue gas and increases the NO reduction efficiency.

1. Introduction

Environmental protection and stringent emission limits both require a significant reduction of nitrogen oxides (NO_x) emissions from industrial boilers as well as waste incineration plants. In recent years, the selective non-catalytic reduction (SNCR) technology, a flue gas treatment method for NO_x emission control, has achieved commercial applications to stationary combustion sources [1]. The technology is attractive due to its simplicity, catalyst-free system, ease of installation on existing plants, applicability to all type of stationary-fired equipments, and lower capital cost [2]. In SNCR the reagent is employed at high temperatures by injection into the combustion chamber. Ammonia (NH_3) and urea ($CO(NH_2)_2$) are common reducing reagents. In waste incineration plants, the reduction of NO_x may range from 60% to 80% under the relevant conditions [3].

Although the technology is considered as simple to install and operate, it has a quite complex chemistry and requires fine operating conditions. In additions, its efficiency of NO_x reduction is specific to each application having different design parameters and operating conditions. The performance of the SNCR process is strongly influenced by several factors including (1) flue gas temperature at the reagent injection zone, (2) flue gas residence time in the relevant temperature range, (3) reagent/NO_x molar ratio (or normalized stoichiometric ratio (NSR) = $2n_{urea}/n_{NO}$, where n_{urea} is the mole of urea in the urea solution and n_{NO} is the mole of NO in the inlet flue gas), and (4) mixing conditions [1]. The optimum temperature is between 900 and 1000 °C in general. With increase of NSR, the reduction efficiency rises up to NSR of about 2 and thereafter generally levels off [3].

Owing to the tightened emissions standards and the desire for the lower cost NO_x emission control, improved computational tools are needed for SNCR design and optimization [4]. Moreover, simulations of chemical process equipments, chemical reactors and a variety of industrial combustion devices using computational fluid dynamics (CFD) tools have gained increasing popularity [5]. CFD has been widely applied to aid the design of SNCR and NO_x emission controlling systems at a full scale [6–10].

In spite of the advantages of computational tools, the implementation of the detailed full chemical kinetics of SNCR [11] on CFD simulations for practical systems is prohibitive from the standpoint of both CPU time and memory. Thus, a reduced chemical kinetic mechanism is widely used [4,7,12–15].

In the present work, the reduced kinetic mechanism with a seven-step global chemistry is implemented on the three-dimensional (3D) turbulent reacting flow CFD model to predict the urea-based SNCR process performance in a municipal solid waste (MSW) incinerator. These kinetics parameters [15] are identified on

* Corresponding author. Tel.: +82 31 670 5207; fax: +82 31 670 5445.
E-mail address: limyi@hknu.ac.kr (Y.-I. Lim).

1385-8947/$ – see front matter © 2009 Elsevier B.V. All rights reserved.
doi:10.1016/j.cej.2009.03.025

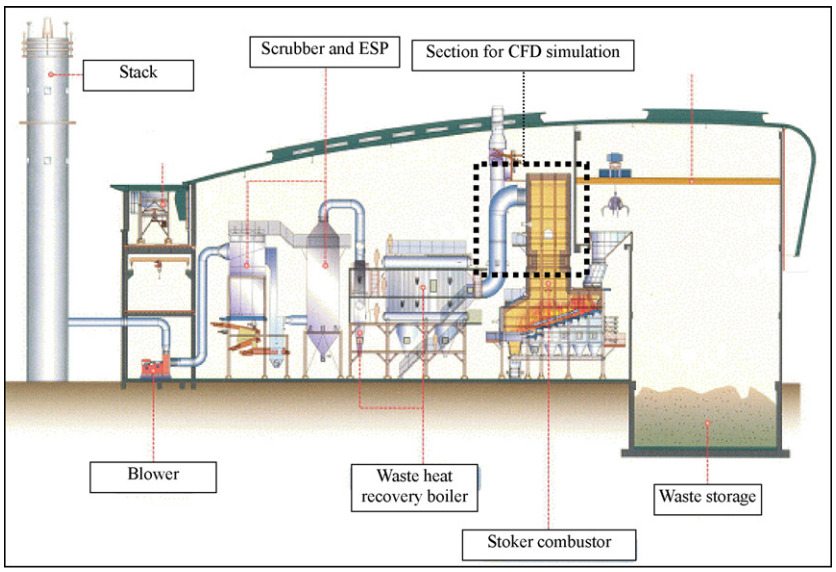

Fig. 1. Schematic diagram of the MSW incineration plant.

the basis of the reduced mechanism of Brouwer et al. [4] and the fully detailed kinetics of Miller and Bowman [11]. The droplet model with the droplet size distribution is also considered to examine the mixing effect of the reagent with the flue gas.

This study aims to (1) apply the turbulent reacting flow CFD model involving the discrete droplet phase to the urea-based SNCR system in a municipal incineration plant, (2) examine the effect of the droplet size distribution on the SNCR performance, (3) compare simulation results of NO and NH_3 concentrations with *in-situ* tests.

2. Incinerator description

The scheme of the municipal solid waste incineration plant considered in this study is presented in Fig. 1. The waste is stored at the waste storage, and then is fed into the stoker combustor for the incineration. The combustor has two chambers: the primary combustor and the secondary combustor. MSW is burned on a sloping and moving grate in the primary combustor. The gas produced from the incineration is treated by a urea-based SNCR process installed in the secondary combustor to reduce the NO_x concentration. Prior to being exhausted to the atmosphere through the stack, the flue gas is conducted through other air pollution control apparatuses such as the scrubber and electrostatic precipitator (ESP). The ash is discharged by the screw conveyor under the fire-grate. The waste heat of flue gas is recovered by the boiler of water-tube type for the steam generation. As indicated in Fig. 1, the section of CFD simulation is bounded within the dashed-line area which belongs to the secondary combustor and the duct, since this study is focused on the SNCR process for NO_x reduction.

The plant capacity was designed for 50 ton/day. The plant data used in this study were obtained from the average values for 20 min, during a stable operation with a medium quality waste. Table 1 shows the proximate and ultimate analyses of the solid waste. The ultimate analysis is shown on the total weight basis, where others (52.14%) mean the ash and moisture.

The plant operating data (temperature, flowrate, and $NO_x/SO_x/CO/O_2$/HCl/dust concentrations) were collected from TMS (telemetry monitoring system) installed for the official atmospheric pollution control. The temperatures were measured just below the neck, at the duct exit and the stack. The average temperatures at the three locations were 1000, 930, and 130 °C, respectively. The sample from the stack was analyzed to measure the flowrate and $NO_x/SO_x/CO/O_2$/HCl/dust concentrations. Under 2 ppm SO_x, less than 3 ppm CO, under 10 ppm HCl, and less than 4 mg/m^3 dust were observed from the TMS data. The average oxygen concentration was 12.1 vol% at the stack. It was expected in that operating period that a stable and quasi-complete combustion took place in the incinerator, because of the low CO concentration and a mild temperature variation (standard deviation of temperature ≈3 °C).

PG-250 (Horiba, Japan) was used to analyze all of the species ($NO_x/SO_x/CO/O_2$/HCl). Ammonia was measured by the NH_3 electrode (Orion 95-12, Thermo-electron Co., USA).

3. CFD modeling

A 3D turbulent reacting flow CFD model [14–15] is applied to the urea-based SNCR process in the incinerator plant. Fluent (Fluent Inc., USA), one of the CFD codes, is used for the CFD model calculation on a personal computer (2.66 GHz quadra-core CPU and 8 GB RAM).

Below are the geometry/mesh structures, the boundary condition, and the CFD model with chemical reactions described. In addition, a discrete droplet phase model with the nonuniform droplet size is mentioned shortly.

Table 1
Proximate and ultimate analyses of the municipal solid waste of medium quality.

Proximate analysis (%)	High quality	Medium quality	Low quality
Moisture	24.72	38.59	51.39
Combustibles	58.74	47.86	38.22
Ash	16.54	13.55	10.39
Total	100.00	100.00	100.00
Ultimate analysis (dry basis, %)			
Carbon (C)	32.60	25.89	20.67
Hydrogen (H)	4.48	3.62	2.89
Oxygen (O)	20.30	17.18	13.71
Nitrogen (N)	0.60	0.53	0.45
Sulfur (S)	0.16	0.15	0.12
Chlorine (Cl)	0.60	0.49	0.38
Others	41.26	52.14	61.78
Total	100.00	100.00	100.00

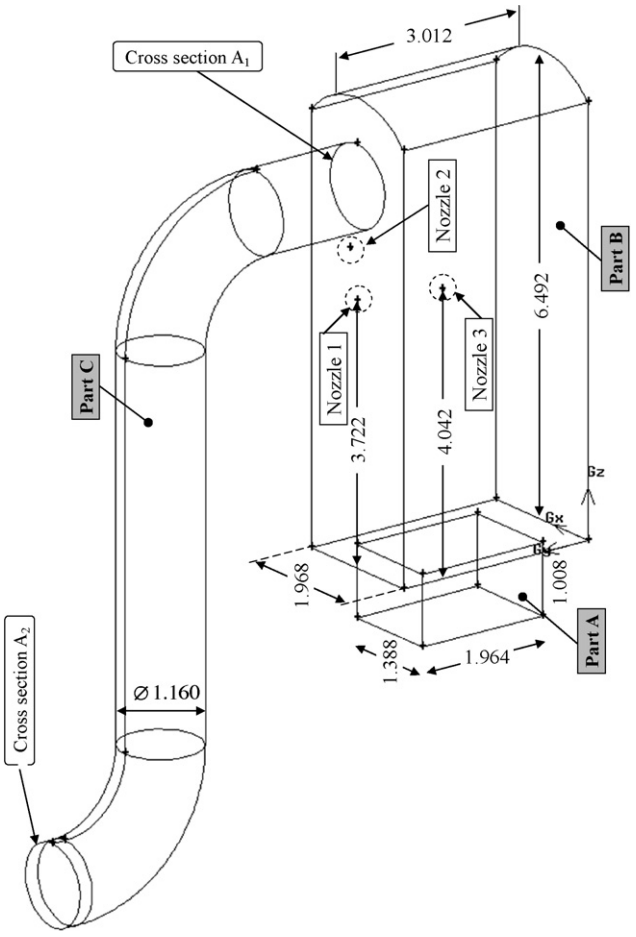

Fig. 2. Geometry of the secondary combustor installed with the SNCR process.

3.1. Geometry and mesh structures

The simulation domain includes three parts: the neck between the secondary and primary combustors (Part A), the secondary combustor where the urea-based SNCR process is installed (Part B), and the duct at the exit of the secondary combustion chamber (Part C). The detailed shape and size of the three parts are shown in Fig. 2.

The main part of the domain is the secondary combustor (Part B). In this chamber, three nozzles are used to inject urea solution for NO_x reduction. As shown in Fig. 2, Nozzle 1 is installed on the front wall of the incinerator. Nozzles 2 and 3 are located on the opposite side of the wall. The three nozzles have the same shape and size. The inner diameter (ID) of each nozzle tip is 0.005 m and the nozzle tip pushes out from the wall by 0.01 m.

The mesh of the whole domain is created by only hexahedrons in order to improve the accuracy of the numerical simulation. The grid dependence is taken into account by testing two cases with the cell numbers of about 380,000 and 490,000. Since there was no significant difference between the two mesh structures in the flow and mass characteristics (velocity, temperature, and concentration), the coarse grid structure (390,000 hexahedral cells) was selected to save the computational time.

3.2. Boundary conditions

The flue gas produced from the waste combustion at the primary combustor is mixed with the excess air before entering into the secondary combustor so that the volatile components can be burnt completely. In the simulation, the combustion of the combustibles is assumed to be complete. Thus, the flue gas entering to the secondary combustor is a mixture of NO, CO_2, H_2O, O_2 and balanced N_2. For the medium quality waste combustion, Table 2 reports the inlet conditions of the main gas flow, urea solution, and atomizing air.

The main gas flowrate is about 13,000 Nm^3/h (dry basis). The inlet concentrations of NO and O_2 are 150 ppm and 12 vol%, respectively. Urea–water solution (4 wt%) was injected into the secondary chamber through the three nozzles with a volume flowrate of 0.115 Nm^3/h equivalent to NSR = 1.8 at 2 atm. Since urea is assumed to be instantaneously decomposed above 850 °C [15], the equimolar flowrate of ammonia (NH_3) and isocyanic acid (HNCO) instead of urea is set to the boundary condition. Urea solution was atomized by the compressed air (50 Nm^3/h) at 100 °C and 25 atm. The initial velocities of the three inlet flows were calculated at the given temperature and pressure.

Wall temperatures along Parts A and B in Fig. 2 decrease because of heat loss to surrounding. The decreasing wall boundary temperatures were approximated by the following linear equations:

$$T_{W,A}(z_A) = 830 - 29.8z_A, \quad 0 \le z_A \le 1\,\text{m} \tag{1}$$

$$T_{W,B}(z_B) = 800 - 15.4z_B, \quad 0 \le z_B \le 6.5\,\text{m} \tag{2}$$

where $T_{W,A}$ (°C) and $T_{W,B}$ (°C) are the wall temperatures at Parts A and B, respectively. z (m) is the height of each part. Sine the heat loss of the neck (Part A) is higher than that of the chamber (Part B) because of higher velocity and overall heat transfer coefficient, the wall temperature quenching rate of Part A (30 °C/m) is about twice higher than that of Part B (15 °C/m). In convenience, the wall temperature of the duct kept constant at $T_{W,C}$ = 660 °C. Those quenching

Table 2
Boundary conditions of species at the inlets.

	Species	Volume flowrate (Nm^3/h)	Mole flowrate (kmol/h)	Mass flowrate (kg/s)	Velocity (m/s)	Temperature (°C)	Pressure (atm)
Combustor inlet	NO	1.91265	0.085386	0.000712	6	1000	1
	CO_2	790.562	35.293	0.4314			
	O_2	1,530.120	68.309	0.6072			
	N_2	10,428.405	465.554	3.6210			
	Total	**12,751**	**569.241**	**4.6602**			
Urea solution (4 wt%)	Urea solution	0.115			87	100	2
	Urea		0.077				
	H_2O		6.148	0.031			
	NH_3		0.077	0.00036			
	HNCO		0.077	0.00092			
	Total	**0.115**	**6.301**	**0.032**			
Atomizing air	O_2	10.50	0.469	0.0042	87	100	25
	N_2	39.50	1.763	0.0137			
	Total	**50.0**	**2.232**	**0.0179**			

Table 3
Model parameters and constants used in this study.

Models	Parameters and constants		
		Turbulent intensity, I (%)	Hydraulic diameter, D_H (m)
k–ε model	Combustor inlet	8	1.627
	Nozzle inlets	10	0.005
	Combustor outlet	10	1.16
	Volume fraction constant, C_ξ (–)	Time scale constant, C_τ (–)	
EDC model	2.1377	0.4083	
Droplet model	Mean diameter, d_{mean} (μm)	Spread parameter, q (–)	
Uniform	45	–	
Rosin–Rammler	45	3.0	

rates were estimated in the iterative way to fit the temperature plant data.

3.3. Turbulent reacting flow CFD model

The physical and chemical phenomena occurring inside the secondary combustion chamber include: (1) turbulence, (2) chemical species transport and reaction, and (3) interaction between the bulk gas phase and reagent droplet phase.

The turbulent reacting flow CFD model used in this study involves the Navier–Stokes equation, the standard k–ε model, the eddy-dissipation concept (EDC) model, the reduced chemical kinetics model, and the droplet model with uniform/nonuniform droplet sizes [14,15]. Table 3 shows the model parameters and constants used in this study.

The turbulent intensity (I) is defined as the ratio of the root-mean-square of the velocity fluctuations (u') to the mean flow velocity (u_{avg}). The turbulent intensity at the core of a fully developed duct flow can be estimated from the following formula derived from an empirical correlation [16]:

$$I = \frac{\sqrt{(u')^2}}{\sqrt{u_{avg}^2}} \approx 0.16(Re)^{-1/8} \quad (3)$$

where Re is the Reynolds number. The hydraulic diameters (D_H) of the inlet zones given in Table 3 are calculated by the following equation:

$$D_H = \frac{4A}{P} \quad (4)$$

where A is the cross-sectional area and P is the wetted perimeter of the cross-section.

To consider the turbulent reacting CFD with multi-step chemical reactions, the eddy-dissipation-concept was used [1,7,16]. The constants of volume fraction (C_ξ) and time scale (C_τ) of the EDC model were set by default (see Table 3). The thermal radiation was not considered in this CFD simulation, because it affected little the temperature profile inside the second combustor.

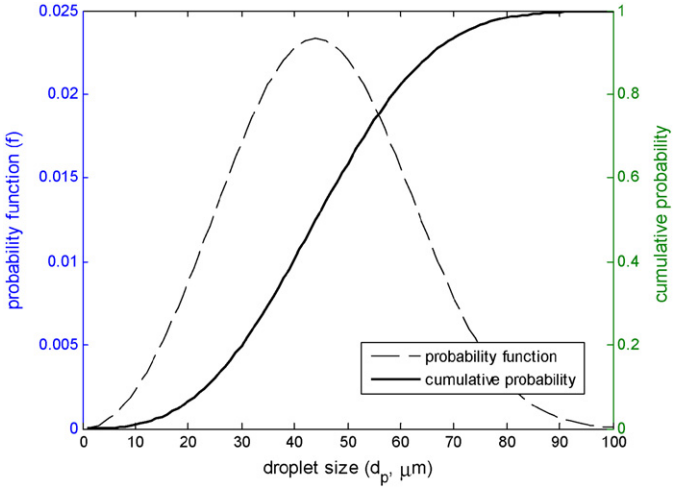

Fig. 3. Droplet size probability function of Rosin–Rammler and its cumulative probability within the range of 1 μm ≤ d ≤ 100 μm.

One of the important parameters in calculating and modeling an atomization process is the droplet size distribution [17,18], which influences the evaporation rate and the mixing between the droplet phase and bulk phase. According to the empirical equation of Boll et al. [17] for the air/water system ($4.22 \times 10^{-2} + 5.77 \times 10^{-3}(1000Q_L/Q_G)^{1.922}/v_G^{1.602}$, where Q_L/Q_G is the liquid to gas volume flowrate ratio and v_G (m/s) is the gas velocity at the point of liquid injection), the mean droplet size was estimated to 55 μm for this atomizing nozzle injection system. Considering that the nozzle tip is exposed in the high temperature range (900–1000 °C), the mean droplet size was set to 45 μm.

The uniform and nonuniform droplet size distributions were applied to examine their mixing between the bulk phase (flue gas) and droplet phase (reagents). The Rosin–Rammler distribution has been used to represent the nonuniform size distribution of liquid droplets produced by atomization [18]. The probability density function of Rosin–Rammler is expressed as follows [18]:

$$f(d) = q\frac{d^{q-1}}{X^q}\exp\left[-\left(\frac{d}{X}\right)^q\right] \quad (5)$$

$$X = \frac{d_{mean}}{\Gamma(1/q+1)} \quad (6)$$

where q is the dimensionless dispersion coefficient or spread parameter, d_{mean} is the arithmetic mean diameter of the droplets and Γ is the Gamma function.

The typical range of the spread coefficient (q) for the liquid spray droplets is from 1.5 to 4.5. The distribution of the spray droplets with high velocity is well fit to the narrow spread parameter (or large spread coefficient) [16,18]. Thus, the narrow spread parameter (q = 3) was used in this study (see Table 3). For q = 3, Fig. 3 shows the droplet size probability and its cumulative probability along the droplet size (d) between 1 and 100 μm.

Table 4
Reduced kinetics parameters used in this study.

No.	Reaction	Pre-exponent (A_i), $\left[\frac{1}{sK^b}\right.$ or $\left.\frac{m^3}{sK^b\,kmol}\right]$	Temperature exponent (b_i), (–)	Activation energy ($E_{a,i}$), (J/kmol)
1	$NH_3 + NO \rightarrow N_2 + H_2O + H$	2.13×10^1	5.3	2.43×10^8
2	$NH_3 + O_2 \rightarrow NO + H_2O + H$	8.83×10^3	7.65	5.86×10^8
3	$HNCO + M \rightarrow H + NCO + M$	1.39×10^{13}	0.85	3.45×10^8
4	$NCO + NO \rightarrow N_2O + CO$	2.26×10^{15}	0.0	-2.60×10^7
5	$NCO + OH \rightarrow NO + CO + H$	3.68×10^9	0.0	0.0
6	$N_2O + OH \rightarrow N_2 + O_2 + H$	8.60×10^4	0.0	8.37×10^7
7	$N_2O + M \rightarrow N_2 + O + M$	8.50×10^7	0.0	3.39×10^8

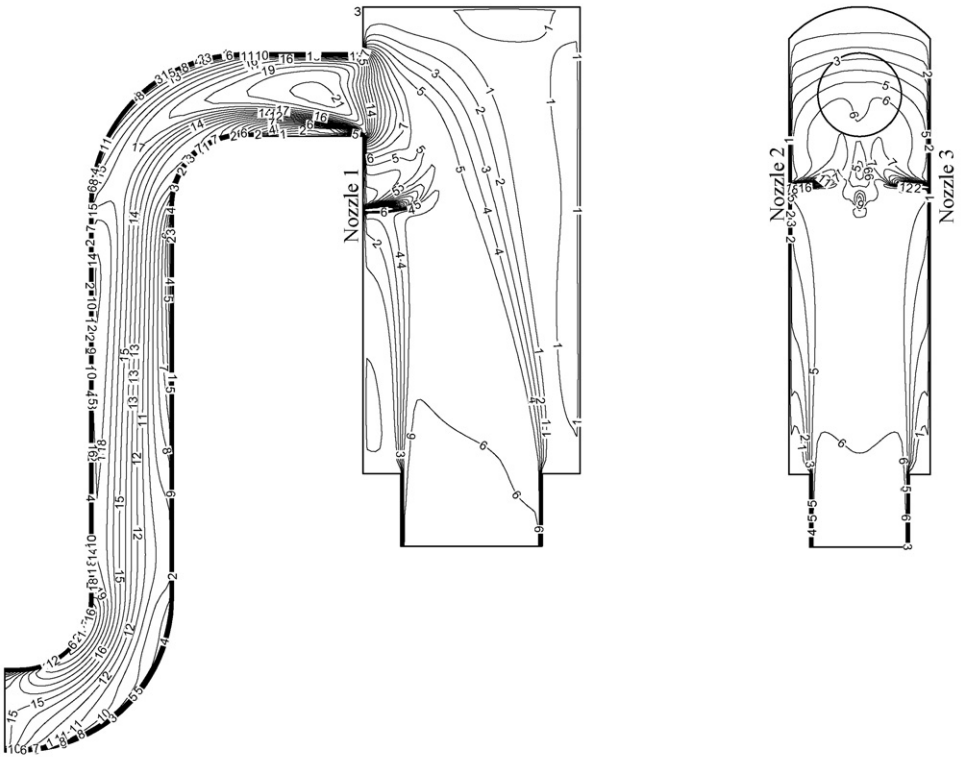

(a) Side view of the whole domain. (b) Front view of the whole domain.

Fig. 4. Contours of velocity inside the secondary combustor. (a) Side view of the whole domain. (b) Front view of the whole domain.

The kinetics parameters of the seven-step reaction mechanism [4] were adjusted to be available under the conditions of a low CO concentration (under 10 ppm) and high excess air (10–12%) which are actual incinerator operating conditions [15]. The reduced kinetics parameters used in this study are shown in Table 4. The each reaction rate (k_i) is expressed as follows:

$$k_i = A_i T^{b_i} e^{-E_{a,i}/RT}, \quad i = 1, 2, \ldots, 7 \tag{7}$$

where A_i is the pre-exponential factor, b_i the temperature exponent and $E_{a,i}$ the activation energy (J/kmol) of reaction i. R is the gas constant (R = 8314.4 J/kmol/K). Since the reduced kinetic model considers the reactions between the reagents (NH_3 and HNCO) and nitrogen oxide (NO) without additives, effects of the HCl gas and flying ash (inorganic and metals) on the SNCR kinetics are ignored.

4. Results and discussions

In this section, the CFD simulation results are compared to the on-site experimental data. Velocity and temperature profiles obtained from the 3D turbulent reacting flow CFD model are presented and the effect of the droplet size distribution on NO reduction is examined.

Table 5 compares *in-situ* experiments with both the SNCR kinetics model and CFD simulation results. The error bound of the on-site measurements is ±8 °C for temperature (±5 °C instrumental error and 3 °C in standard deviation of operating temperature), ±11 ppm and ±6 ppm for NO inlet and outlet concentrations, respectively, which were caused mainly by the NO analyzer instrumental error (5%) and the operational fluctuation (standard deviation = 4 ppm). The outlet concentrations of NO and NH_3 in Table 5 come from the TMS data measured at the stack. Since the flue gas from the duct is quenched rapidly from 930 to 220 °C, it is assumed that further NO reduction does not occur after the duct exit. In fact, no significant difference between the concentrations at the two locations (duct exit and stack) was observed in several on-site measurements.

The kinetics model result was obtained under the isothermal homogeneous perfect mixing condition, where the SNCR seven equations (Eq. (7)) were solved for a given residence time (0.17 s) at T = 980 °C and NSR = 1.8. The SNCR residence time was estimated under the assumption that the reagent trajectory length was about 1.0 m at T = 980 °C. Therefore, in this kinetic model, the major SNCR process parameters such as reactant mixing, reaction temperature and residence time [15] do not well reflect the real situations in comparison with the CFD model.

Table 5
Kinetics model and CFD simulation results in comparison with the on-site test.

	On-site experiment	SNCR kinetics model	CFD simulation	
			Uniform droplet size	Nonuniform droplet size
Inlet temperature (°C)	1000 ± 8	980	1000	1000
Outlet temperature (°C)	930 ± 8	980	923 (−1%)[a]	923 (−1%)[a]
NO inlet (ppm)	150 ± 11	150	150	150
NO outlet (ppm)	45 ± 6	9 (−80%)[a]	58 (29%)[a]	51 (13%)[a]
NH_3 slip (ppm)	Under 5	19	1.4	1.5

[a] Error(%) = $\frac{\text{simulation} - \text{experiment}}{\text{experiment}} \times 100$.

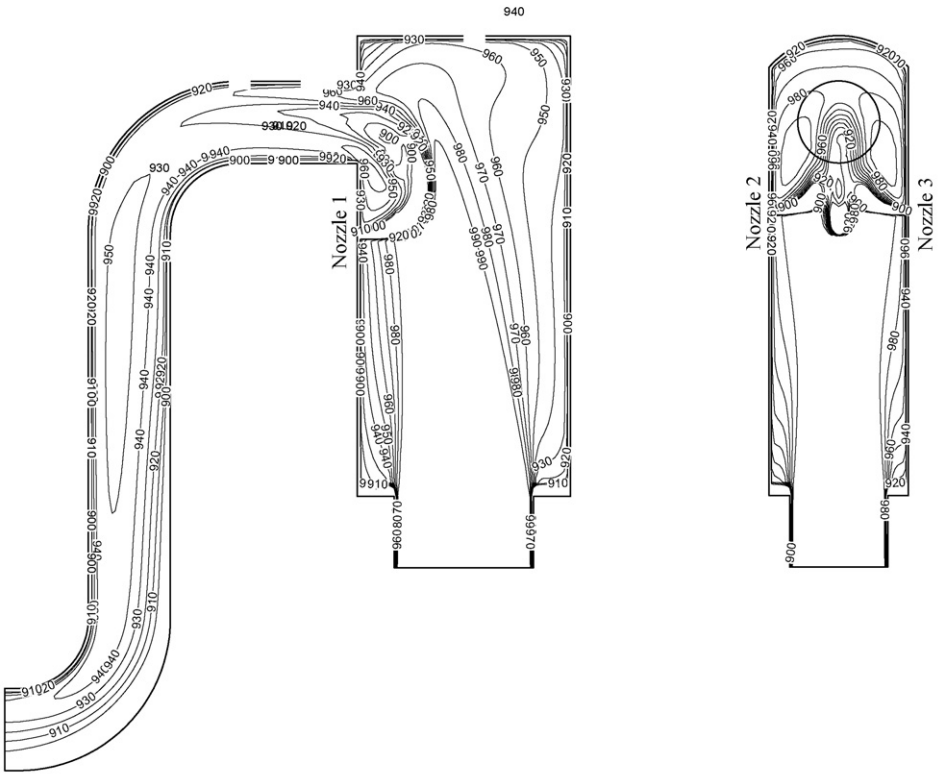

(a) Side view of the whole domain. (b) Front view of the whole domain.

Fig. 5. Contours of temperature inside the secondary combustor. (a) Side view of the whole domain. (b) Front view of the whole domain.

As expected, the SNCR kinetics model under an idealized situation produces a higher NO_x reduction (94%) and a higher NH_3 slip (19 ppm) than the experiment and CFD simulation. As the lower NO reduction the higher ammonia slip, the experimental value of ammonia slip (under 5 ppm) is exceptional. It may result from both the second reaction (ammonia oxidation) of Table 4 over 980 °C and uncaught reactions such as an ammonium chloride formation. Ammonia slip in the CFD simulation is also relatively low. At a chemical kinetic point of view from Table 4, it can be explained that the second reaction (NO formation from NH_3) over 980 °C becomes activated and considerable NH_3 is reduced (see also Fig. 4 in Nguyen et al. [15]).

4.1. Velocity and temperature contours

The velocity contour inside the secondary combustor is shown in Fig. 4. The inlet velocity is about 6 m/s. Small eddy flows are observed at the corners of the secondary combustor, as shown in Fig. 4(a) of the side view. The front view of the secondary combustor in Fig. 4(b) shows well the velocity filed disturbance around Nozzles 2 and 3.

In Fig. 5, the temperature contour of the whole computational domain is shown. The main gas flow enters to the secondary combustor at $T = 1000$ °C. The side view in Fig. 5(a) shows the temperature profile around the front nozzle (Nozzle 1). The temperature decreases along the height and low temperature regions are observed near the nozzles because of the urea solution injection at 100 °C (see Fig. 5(a and b)). In Table 5, the outlet temperature obtained from CFD simulation is compared with on-site experimental data. For both the uniform droplet size distribution (45 μm) and the nonuniform distribution ($d_{mean} = 45$ μm and $q = 3$), the error between the experiment and simulation is 1%, which belongs to the error bound of experimental temperature. It is thus confirmed that the wall boundary temperature specified by Eqs. (1) and (2) is reasonably approximated.

4.2. NO concentration according to droplet size distribution

The uniform droplet size distribution (45 μm) and the nonuniform distribution ($d_{mean} = 45$ μm and $q = 3$) are taken into account to examine their mixing effects on the NO reduction efficiency.

Fig. 6 shows NO concentration contours near Nozzle 1 for the uniform and nonuniform droplet sizes. In the CFD simulation result, the outlet NO reduction is higher for the nonuniform droplet size than for the uniform one, as also indicated in Table 5. The NO reduction percentage is 70% by the on-site experiment and 66% by the simulation with the nonuniform droplet size. The error between the on-site experiment and simulation with the nonuniform distribution of droplet size is 13%. The result from the nonuniform droplet size reduces the NO concentration by 7 ppm more, compared to the uniform one. Since the nonuniform droplet size is distributed broadly from 1 to 100 μm, the bulk flow mixing with the reagent may be promoted and the high NO reduction is achieved.

Fig. 7 shows the front view of the NO concentration profile around Nozzle 2 and 3 for the uniform and nonuniform droplet sizes. It can be observed that the nonuniform droplet size distribution ($1\ \mu m \le d \le 100\ \mu m$) enhances NO reduction, broadening an effective mixing zone for NO reduction. However, in order to measure quantitatively the mixing effect of the droplet distribution, a dimensionless concentration dispersion number (N_{NO}) is proposed as follows:

$$N_{NO} = \frac{\mu_{NO}}{\sigma_{NO}} \tag{8}$$

where μ_{NO} and σ_{NO} are the mean and the standard deviation of NO concentration at a cross-sectional area perpendicular to the bulk

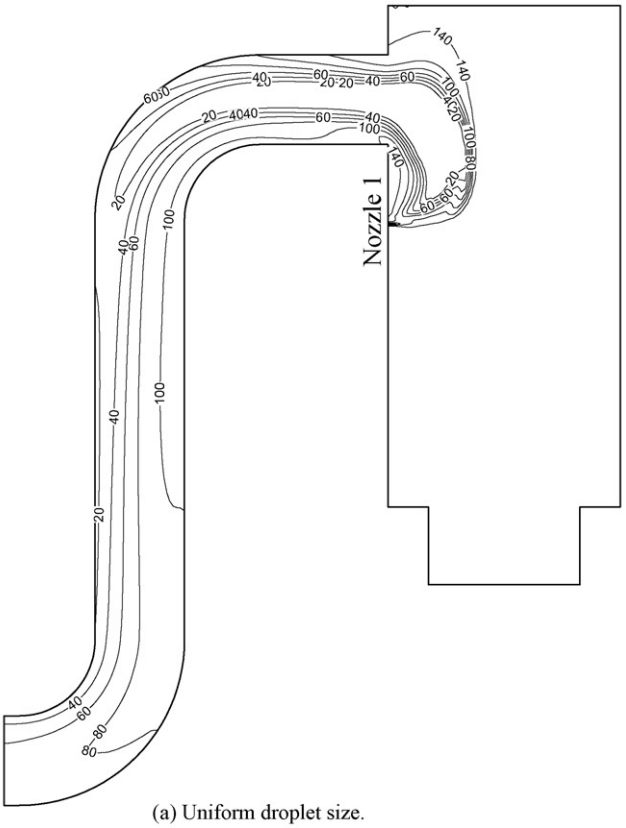

(a) Uniform droplet size.

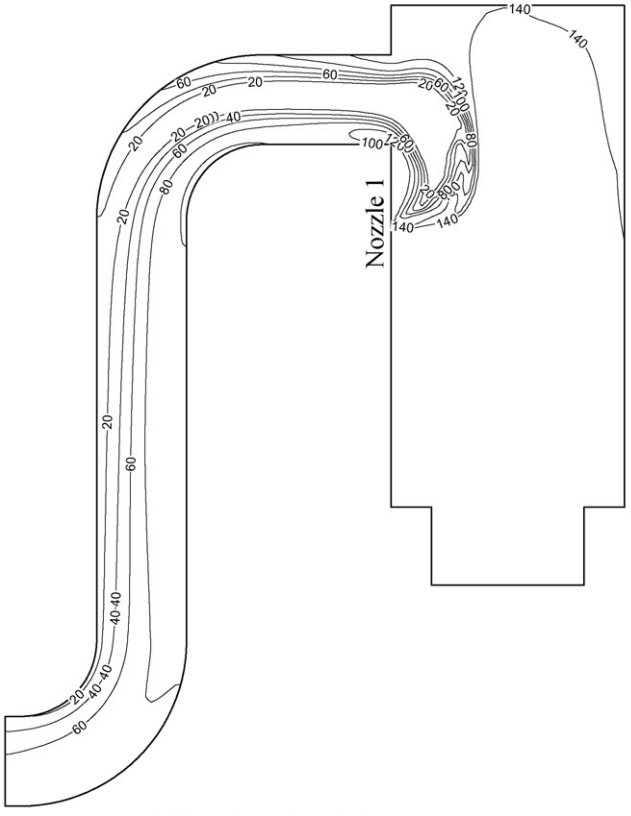

(b) Nonuniform droplet size.

Fig. 6. Contours of NO concentration around Nozzle 1. (a) Uniform droplet size. (b) Nonuniform droplet size.

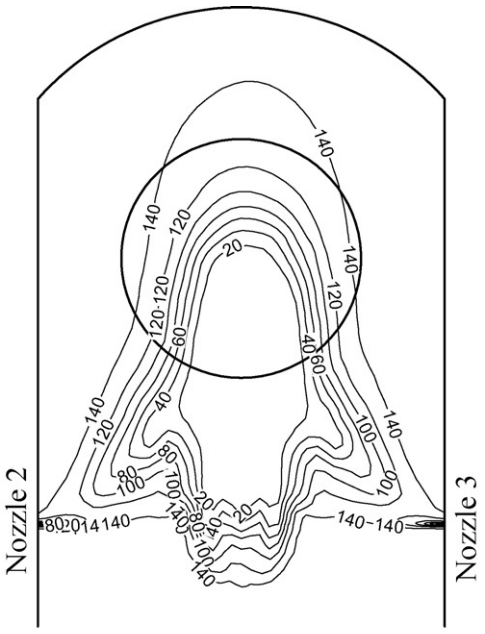

(a) Uniform droplet size.

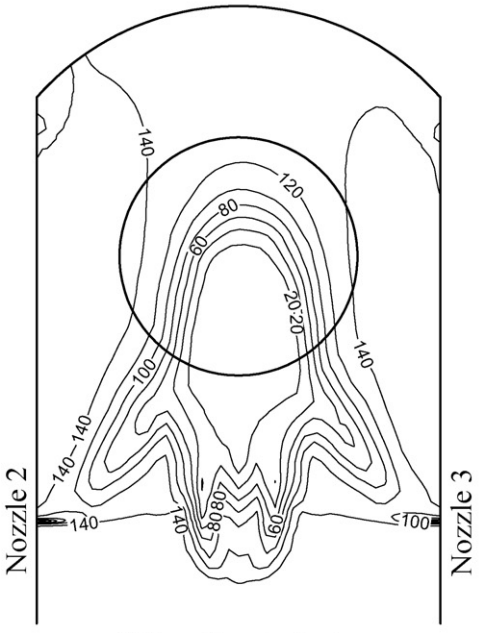

(b) Nonuniform droplet size.

Fig. 7. Contours of NO concentration around Nozzles 2 and 3. (a) Uniform droplet size. (b) Nonuniform droplet size.

flow direction. Lower the dispersion number, broader the distribution of concentration.

The mixing numbers of NO concentration at cross-sections A_1 and A_2 on the secondary combustor (see Fig. 2) are given in Table 6. It is observed here that, in both two cross-sections A_1 and A_2, the dispersion number (N_{NO}) of nonuniform distribution is lower than that of the uniform one. As a result, the nonuniform distribution of droplets improves the mixing with the reagent and bulk flue gas, and results in the lower dispersion numbers (or broader concentration distributions) and the higher NO reduction.

The droplet size affects the penetration length of droplets and the evaporation time. The uniform droplet distribution has a limited number of droplet trajectories. In contrast, the nonuniform

Table 6
Comparison of NO concentration dispersion number between uniform and the nonuniform droplet size at cross-section A_1 and A_2.

	Cross-section A_1		Cross-section A_2	
	Uniform	Nonuniform	Uniform	Nonuniform
Mean value (μ_{NO}, ppm)	97.03	93.94	58.47	50.72
Standard deviation (σ_{NO}, ppm)	46.15	45.58	10.71	10.97
Dispersion number (N_{NO})	2.10	2.06	5.46	4.62

droplets have much various trajectories, which is more realistic. The various penetration lengths (or trajectories) enhance mixing between the reagent and flue gas, and increase the NO reduction efficiency.

5. Conclusions

A 3D turbulent reacting flow CFD model involving SNCR reaction kinetics and a discrete droplet phase with the uniform or nonuniform droplet size is applied to a full scale SNCR system at a MSW incineration plant. The velocity, temperature and species concentrations in the SNCR zone are predicted. The error between on-site test and CFD simulation with the nonuniform droplet size is about 1% for temperature and 13% for NO concentration. The NO reduction percentage is 70% in on-site experiment and 66% in simulation with the nonuniform droplet size.

The effect of the droplet size distribution on SNCR performance is examined by means of CFD simulation. The nonuniform distribution of the reagent droplets provides a better efficiency of NO_x reduction than the uniform one. The mixing between the reagent and flue gas is examined on the basis of the dimensionless dispersion number of NO concentration. It is found that a low dispersion number indicates a high mixing ability and a high efficiency of NO_x reduction.

Acknowledgements

This study is supported by Korea Ministry of Environment as "The Eco-technopia 21 Project". We thank the Byucksan Engineering Co., Ltd. (BEC) for the supply of the plant diagrams of the municipal incinerator. We appreciate to Nonsan Green Environment Co. for the helpful discussion and providing precious plant data.

References

[1] S. Zandaryaa, R. Gavasci, F. Lombardi, A. Fiore, Nitrogen oxides from waste incineration: control by selective non-catalytic reduction, Chemosphere 42 (2001) 491–497.
[2] M. Tayyeb Javed, N. Irfan, B.M. Gibbs, Control of combustion-generated nitrogen oxides by selective non-catalytic reduction, J. Environ. Manage. 83 (2007) 251–289.
[3] J. Furrer, H. Deuber, H. Hunsinger, S. Kreisz, A. Linek, H. Seifert, J. Stohr, R. Ishikawa, K. Watanabe, Balance of NH_3 and behavior of polychlorinated dioxins and furans in the course of the selective non-catalytic reduction of nitric oxide at the TAMARA waste incineration plant, Waste Manage. 18 (1998) 417–442.
[4] J. Brouwer, M.P. Heap, D.W. Pershing, P.J. Smith, A model for prediction of selective non-catalytic reduction of nitrogen oxides by ammonia, urea and cyanuric acid with mixing limitations in the presence of CO, in: Twenty-Sixth Symposium (International) on Combustion/The Combustion Institute, 1996, pp. 2117–2124.
[5] M.S. Skjoth-Rasmunssen, O. Holm-Christensen, M. Ostberg, T.S. Christensen, T. Johannessen, A.D. Jensen, P. Glarborg, H. Livbjerg, Post-processing of detailed chemical kinetic mechanisms onto CFD simulations, Comput. Chem. Eng. 28 (2004) 2351–2361.
[6] B.R. Stanmore, S.P. Visona, Prediction of NO emissions from a number of coal-fired power station boilers, Fuel Process. Technol. 64 (2000) 25–46.
[7] X. Han, X. Wei, U. Schnell, Klaus R.G. Hein, Detailed modeling of hybrid reburn/SNCR processes for NO_x reduction in coal-fired furnaces, Combust. Flame 132 (2003) 374–386.
[8] H.-S. Kim, M.-S. Shin, D.-S. Jang, T.-I. Ohm, Numerical of SNCR application to a full-scale stoker incinerator at Daejon 4th industrial complex, Appl. Therm. Eng. 24 (2004) 2117–2129.
[9] J. Chacon, J.M. Sala, J.M. Blanco, Investigation on the design and optimization of a low NO_x-CO emission burner both experimentally and through computational fluid dynamics (CFD) simulations, Energy Fuel 21 (2007) 42–58.
[10] L.I. Diez, C. Cortes, J. Pallares, Numerical investigation of NO_x emissions from a tangentially-fired utility boiler under conventional and overfire air operation, Fuel 87 (2008) 1259–1269.
[11] J.A. Miller, C.T. Bowman, Mechanism and modeling of nitrogen chemistry in combustion, Prog. Energy Combust. Sci. 15 (1989) 287–338.
[12] M.A. Cremer, C.J. Montgomery, D.H. Wang, M.P. Heap, J.-Y. Chen, Development and implementation of reduced chemistry for CFD modeling of selective non-catalytic reduction, in: Proceeding of the Combustion Institute, 28, 2000, pp. 2427–2434.
[13] C.J. Montgomery, D.A. Swensen, T.V. Harding, M.A. Cremer, M.J. Bockelie, A computational problem solving environment for creating and testing reduced chemical kinetic mechanisms, Adv. Eng. Software 33 (2002) 59–70.
[14] D.B.T. Nguyen, T.-H. Kang, Y.-I. Lim, S.-J. Kim, W.-H. Eom, K.-S. Yoo, Computational fluid dynamics (CFD) simulation for a pilot-scale selective non-catalytic reduction (SNCR) process using urea solution, Korean Chem. Eng. Res. 46 (2008) 922–930.
[15] D.B.T. Nguyen, Y.-I. Lim, S.-J. Kim, W.-H. Eom, K.-S. Yoo, Experiment and CFD simulation of urea-based selective non-catalytic reduction (SNCR) in a pilot scale flow reactor, Energy Fuel 22 (2008) 3864–3876.
[16] Fluent user guide, Fluent 6.3 Documentation, Fluent Inc., 2007.
[17] D.F. Alonso, J.A.S. Goncalves, B.J. Azzopardi, J.R. Coury, Droplet size measurements in Venturi scrubbers, Chem. Eng. Sci. 56 (2001) 4901–4911.
[18] S.S. Yoon, H.Y. Kim, J.C. Hewson, Effect of initial conditions of modeled PDFs on droplet characteristics for coalescing and evaporating turbulent water used in fire suppression applications, Fire Saf. J. 42 (2007) 393–406.